

## LOCALIZATION AND BROADBAND FOLLOW-UP OF THE GRAVITATIONAL-WAVE TRANSIENT GW150914

THE LIGO SCIENTIFIC COLLABORATION AND THE VIRGO COLLABORATION,  
THE AUSTRALIAN SQUARE KILOMETER ARRAY PATHFINDER (ASKAP) COLLABORATION, THE BOOTES COLLABORATION,  
THE DARK ENERGY SURVEY AND THE DARK ENERGY CAMERA GW-EM COLLABORATIONS, THE *Fermi* GBM COLLABORATION,  
THE *Fermi* LAT COLLABORATION, THE GRAVITATIONAL WAVE INAF TEAM (GRAWITA), THE *INTEGRAL* COLLABORATION,  
THE INTERMEDIATE PALOMAR TRANSIENT FACTORY (IPTF) COLLABORATION, THE INTERPLANETARY NETWORK,  
THE J-GEM COLLABORATION, THE LA SILLA–QUEST SURVEY, THE LIVERPOOL TELESCOPE COLLABORATION,  
THE LOW FREQUENCY ARRAY (LOFAR) COLLABORATION, THE MASTER COLLABORATION, THE MAXI COLLABORATION,  
THE MURCHISON WIDE-FIELD ARRAY (MWA) COLLABORATION, THE PAN-STARRS COLLABORATION,  
THE PESSTO COLLABORATION, THE PI OF THE SKY COLLABORATION, THE SKYMAPPER COLLABORATION,  
THE *Swift* COLLABORATION, THE TAROT, ZADKO, ALGERIAN NATIONAL OBSERVATORY, AND C2PU COLLABORATION,  
THE TOROS COLLABORATION, AND THE VISTA COLLABORATION

See the Supplement, [Abbott et al. 2016g](#), for the full list of authors.

(Received 2016 February 29; Accepted 2016 April 26; Published 2016 July 20)

### ABSTRACT

A gravitational-wave (GW) transient was identified in data recorded by the Advanced Laser Interferometer Gravitational-wave Observatory (LIGO) detectors on 2015 September 14. The event, initially designated G184098 and later given the name GW150914, is described in detail elsewhere. By prior arrangement, preliminary estimates of the time, significance, and sky location of the event were shared with 63 teams of observers covering radio, optical, near-infrared, X-ray, and gamma-ray wavelengths with ground- and space-based facilities. In this Letter we describe the low-latency analysis of the GW data and present the sky localization of the first observed compact binary merger. We summarize the follow-up observations reported by 25 teams via private Gamma-ray Coordinates Network circulars, giving an overview of the participating facilities, the GW sky localization coverage, the timeline and depth of the observations. As this event turned out to be a binary black hole merger, there is little expectation of a detectable electromagnetic (EM) signature. Nevertheless, this first broadband campaign to search for a counterpart of an Advanced LIGO source represents a milestone and highlights the broad capabilities of the transient astronomy community and the observing strategies that have been developed to pursue neutron star binary merger events. Detailed investigations of the EM data and results of the EM follow-up campaign are being disseminated in papers by the individual teams.

*Keywords:* gravitational waves; methods: observational

### 1. INTRODUCTION

In 2015 September, the Advanced Laser Interferometer Gravitational-wave Observatory (LIGO; [Aasi et al. 2015](#)) made the first direct detection of an astrophysical gravitational-wave (GW) signal that turned out to be from a binary black hole (BBH) merger. The LIGO Hanford and Livingston sites are the first two nodes of a growing global network of highly sensitive GW facilities, soon to include Advanced Virgo ([Acernese et al. 2015](#)), KAGRA, and LIGO–India. Some of the most promising astrophysical sources of GWs are also expected to produce broadband electromagnetic (EM) emission and neutrinos. This has created exciting new opportunities for joint broadband EM observations and multi-messenger astronomy.

In a compact binary coalescence (CBC) event, a tight binary comprised of two neutron stars (NSs), two black holes (BHs),

or a NS and a BH experiences a runaway orbital decay due to gravitational radiation. In a binary including at least one NS—a binary neutron star (BNS) or neutron star–black hole (NSBH) merger—we expect EM signatures due to energetic outflows at different timescales and wavelengths. If a relativistic jet forms, we may observe a prompt short gamma-ray burst (GRB) lasting on the order of one second or less, followed by X-ray, optical, and radio afterglows of hours to days duration (e.g., [Eichler et al. 1989](#); [Narayan et al. 1992](#); [Nakar 2007](#); [Berger 2014](#); [Fong et al. 2015](#)). Rapid neutron capture in the sub-relativistic ejecta (e.g., [Lattimer & Schramm 1976](#)) is hypothesized to produce a kilonova or macronova, an optical and near-infrared signal lasting hours to weeks (e.g., [Li & Paczyński 1998](#)). Eventually, we may observe a radio blast wave from this sub-relativistic outflow, detectable for months to years (e.g., [Nakar & Piran 2011](#)). Furthermore, several seconds prior to or tens of minutes after merger, we may see a coherent radio burst lasting milliseconds (e.g., [Hansen & Lyutikov 2001](#); [Zhang 2014](#)). In short, a NS binary can pro-

duce EM radiation over a wide range of wavelengths and time scales. On the other hand, in the case of a stellar-mass BBH, the current consensus is that no significant EM counterpart emission is expected except for those in highly improbable environments pervaded by large ambient magnetic fields or baryon densities.

The first campaign to find EM counterparts triggered by low-latency GW event candidates was carried out with the initial LIGO and Virgo detectors and several EM astronomy facilities in 2009 and 2010 (Abadie et al. 2012a,b; Evans et al. 2012; Aasi et al. 2014). In preparing for Advanced detector operations, the LIGO and Virgo collaborations worked with the broader astronomy community to set up an evolved and greatly expanded EM follow-up program.<sup>1</sup> Seventy-four groups with access to ground- and space-based facilities joined, of which 63 were operational during Advanced LIGO’s first observing run (O1). Details of the 2009 to 2010 EM follow campaign and changes for O1 are given in Section 1 of the Supplement (Abbott et al. 2016g).

After years of construction and commissioning, the Advanced LIGO detectors at Livingston, Louisiana, and Hanford, Washington, began observing in 2015 September with about 3.5 times the distance reach ( $> 40$  times the sensitive volume) of the earlier detectors. A strong GW event was identified shortly after the pre-run calibration process was completed. Deep analysis of this event, initially called G184098 and later given the name GW150914, is presented in Abbott et al. (2016c) and companion papers referenced therein. In this paper we describe the initial low-latency analysis and event candidate selection (Section 2), the rapid determination of likely sky localization (Section 3), and the follow-up EM observations carried out by partner facilities (Sections 4 and 5). For analyses of those observations, we refer the reader to the now-public Gamma-ray Coordinates Network (GCN) circulars<sup>2</sup> and to a number of recent papers. We end with a brief discussion of EM counterpart detection prospects for future events.

## 2. DATA ANALYSIS AND DISCOVERY

As configured for O1, four low-latency pipelines continually search for transient signals that are coincident in the two detectors within the 10 ms light travel time separating them. Coherent WaveBurst (cWB; Klimenko et al. 2016) and Omicron+LALInference Burst (oLIB; Lynch et al. 2015) both search for unmodeled GW bursts (Abbott et al. 2016d). GST-LAL (Cannon et al. 2012; Messick et al. 2016) and Multi-Band Template Analysis (MBTA; Adams et al. 2015) search specifically for NS binary mergers using matched filtering. Because CBC waveforms can be precisely computed from general relativity, GSTLAL and MBTA are more sensitive to

CBC signals than the burst search pipelines are. All four detection pipelines report candidates within a few minutes of data acquisition.

LIGO conducted a series of engineering runs throughout Advanced LIGO’s construction and commissioning to prepare to collect and analyze data in a stable configuration. The eighth engineering run (ER8) began on 2015 August 17 at 15:00 and critical software was frozen by August 30.<sup>3</sup> The rest of ER8 was to be used to calibrate the detectors, to carry out diagnostic studies, to practice maintaining a high coincident duty cycle, and to train and tune the data analysis pipelines. Calibration was complete by September 12 and O1 was scheduled to begin on September 18. On 2015 September 14, cWB reported a burst candidate to have occurred at 09:50:45 with a network signal-to-noise ratio (S/N) of 23.45 and an estimated false alarm rate (FAR)  $< 0.371 \text{ yr}^{-1}$  based on the available (limited at that time) data statistics. Also, oLIB reported a candidate with consistent timing and S/N. No candidates were reported at this time by the low-latency GSTLAL and MBTA pipelines, ruling out a BNS or NSBH merger.

Although the candidate occurred before O1 officially began, the LIGO and Virgo collaborations decided to send an alert to partner facilities because the preliminary FAR estimate satisfied our planned alert threshold of  $1 \text{ month}^{-1}$ . Although we had not planned to disseminate real-time GCN notices before the formal start of O1, most of the computing infrastructure was in place. Basic data quality checks were done within hours of GW150914; both interferometers were stable and the data stream was free of artifacts (Abbott et al. 2016a). A cWB sky map was available 17 minutes after the data were recorded, and a LALInference Burst (LIB) sky map was available after 14 hr. After extra data integrity checks and an update to the GCN server software, these two sky maps were communicated to observing partners in a GCN circular nearly two days after the event occurred (GCN 18330). Mass estimates were not released in this initial circular, and observers may have assumed the event was associated with a BNS system or a GW burst (e.g., from a nearby core-collapse supernova; SN). The knowledge that GW150914 was consistent with a BBH inspiral and merger was only shared later on October 3 (GCN 18388). Figure 1 shows the chronology of the GW detection alerts and follow-up observations.

The data were re-analyzed offline with two independent matched-filter searches using a template bank that includes both NS binary and BBH mergers. The waveform was confirmed to be consistent with a BBH merger and this information was shared with observers about three weeks after the event (GCN 18388). The FAR was evaluated with the data collected through 20 October, reported to be less than 1 in 100 years (GCN 18851; Abbott et al. 2016b), and ultimately determined to be much lower. The final results of the offline

<sup>1</sup> See program description and participation information at <http://www.ligo.org/scientists/GWEMalerts.php>.

<sup>2</sup> All circulars related to GW150914 are collected at <http://gcn.gsfc.nasa.gov/other/GW150914.gcn3>

<sup>3</sup> All dates and times are in UT.

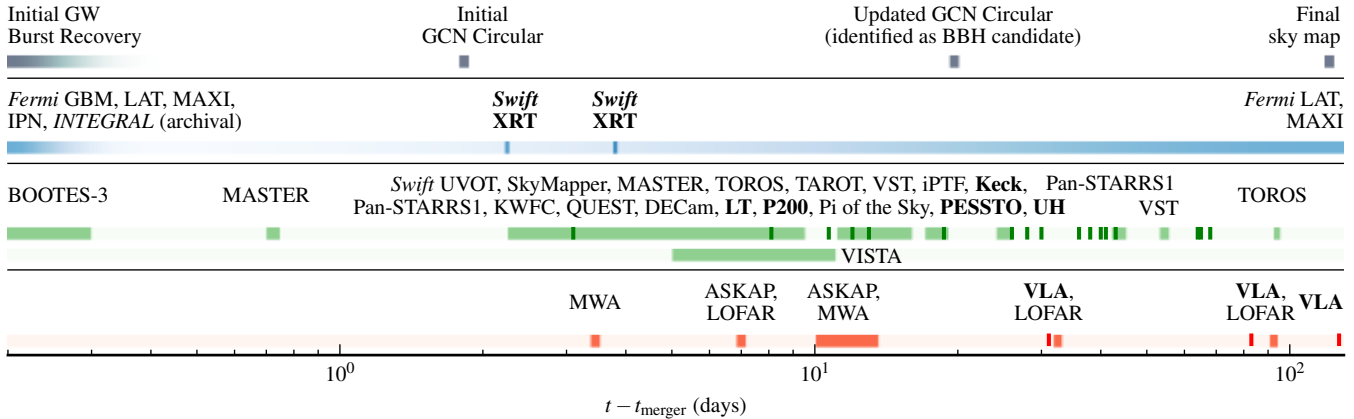


**Figure 1.** Timeline of observations of GW150914, separated by band and relative to the time of the GW trigger. The top row shows GW information releases. The bottom four rows show high-energy, optical, near-infrared, and radio observations, respectively. Optical spectroscopy and narrow-field radio observations are indicated with darker tick marks and boldface text. Table 1 reports more detailed information on the times of observations made with each instrument.

search are reported in [Abbott et al. \(2016c\)](#).

### 3. SKY MAPS

We produce and disseminate probability sky maps using a sequence of algorithms with increasing accuracy and computational cost. Here, we compare four location estimates: the prompt cWB and LIB localizations that were initially shared with observing partners plus the rapid BAYESTAR localization and the final localization from LALInference. All four are shown in Fig. 2.

cWB performs a constrained maximum likelihood estimate of the reconstructed signal on a sky grid ([Klimenko et al. 2016](#)) weighted by the detectors’ antenna patterns ([Essick et al. 2015](#)) and makes minimal assumptions about the waveform morphology. With two detectors, this amounts to restricting the signal to only one of two orthogonal GW polarizations throughout most of the sky. LIB performs Bayesian inference assuming the signal is a sinusoidally modulated Gaussian ([Lynch et al. 2015](#)). While this assumption may not perfectly match the data, it is flexible enough to produce reliable localizations for a wide variety of waveforms, including BBH inspiral-merger-ringdown signals ([Essick et al. 2015](#)). BAYESTAR produces sky maps by triangulating the times, amplitudes, and phases on arrival supplied by all the CBC pipelines ([Singer & Price 2016](#)). BAYESTAR was not available promptly because the low-latency CBC searches were not configured for BBHs; the localization presented here is derived from the offline CBC search. LALInference performs full forward modeling of the data using a parameterized CBC waveform which allows for BH spins and detector calibration uncertainties ([Veitch et al. 2015](#)). It is the most accurate method for CBC signals but takes the most time due to the high dimensionality. We present the same LALInference map as [Abbott et al. \(2016e\)](#), with a spline interpolation proce-

cedure to include the potential effects of calibration uncertainties. The BAYESTAR and LALInference maps were shared with observers on 2016 January 13 (GCN 18858), at the conclusion of the O1 run. Since GW150914 is a CBC event, we consider the LALInference map to be the most accurate, authoritative, and *final* localization for this event. This map has a 90% credible region with area 630 deg<sup>2</sup>.

All of the sky maps agree qualitatively, favoring a broad, long section of arc in the southern hemisphere and to a lesser extent a shorter section of nearly the same arc near the equator. While the majority of LIB’s probability is concentrated in the southern hemisphere, a non-trivial fraction of the 90% confidence region extends into the northern hemisphere. The LALInference sky map shows much less support in the northern hemisphere which is likely associated with the stronger constraints available with full CBC waveforms. The cWB localization also supports an isolated hot spot near  $\alpha \sim 9^{\text{h}}$ ,  $\delta \sim 5^{\circ}$ , where the detector responses make it possible to independently measure two polarization components. In this region, cWB considers signals not constrained to have the elliptical polarization expected from a compact binary merger.

Quantitative comparisons of the four sky maps can be found in section 2 of the Supplement ([Abbott et al. 2016g](#)). The main feature in all of the maps is an annulus with polar angle  $\theta_{\text{HL}}$  determined by the arrival time difference  $\Delta t_{\text{HL}}$  between the two detectors. However, refinements are possible due to phase as well as amplitude consistency and the mildly directional antenna patterns of the LIGO detectors ([Kasliwal & Nissanke 2014](#); [Singer et al. 2014](#)). In particular, the detectors’ antenna patterns dominate the modulation around the ring for un-modeled reconstructions through a correlation with the inferred distance of the source ([Essick et al. 2015](#)). As shown in Fig. 2, the algorithms all infer polar angles that are consistent at the  $1\sigma$  level.

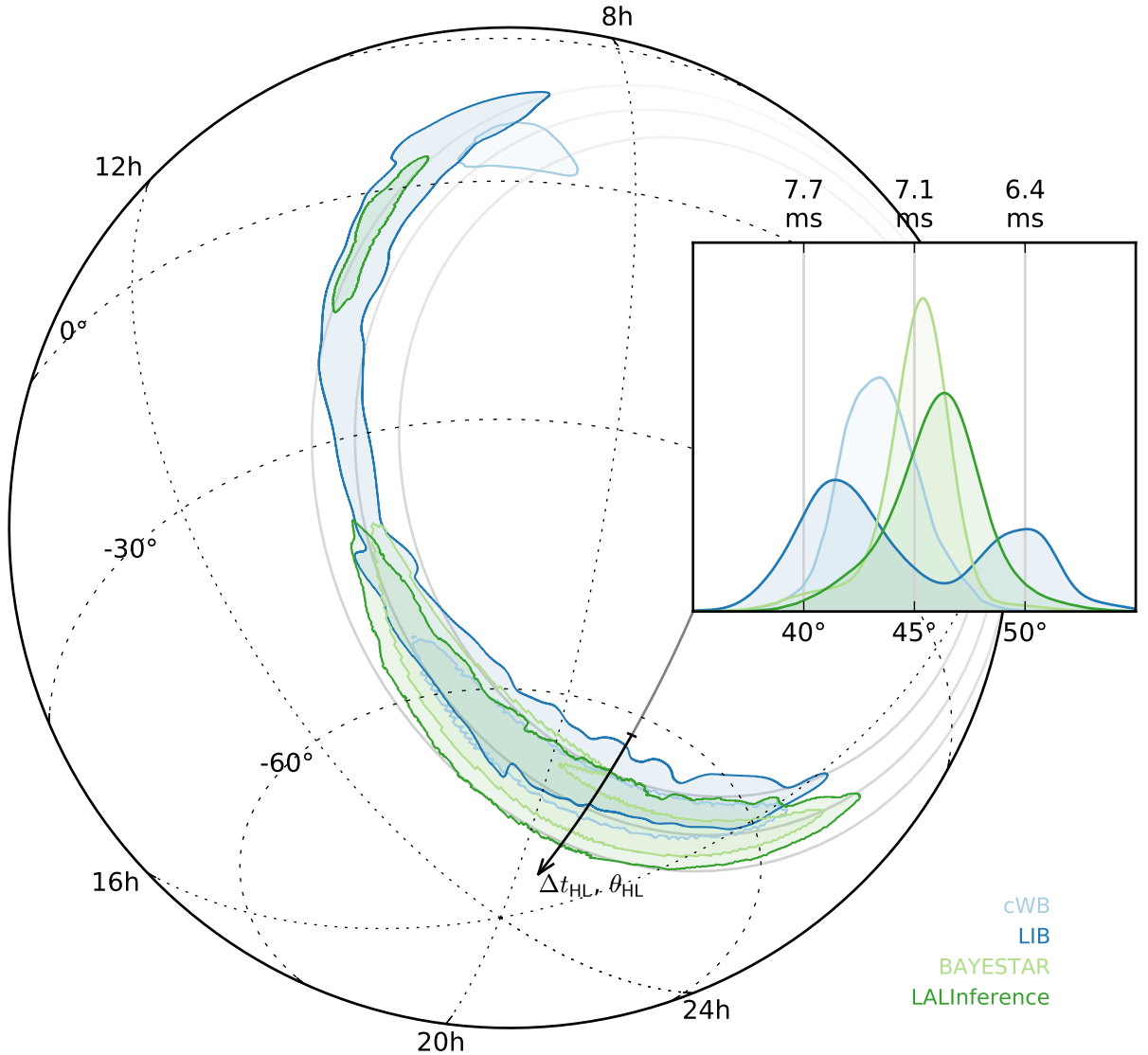


**Figure 2.** Comparison of different GW sky maps, showing the 90% credible level contours for each algorithm. This is an orthographic projection centered on the centroid of the LIB localization. The inset shows the distribution of the polar angle  $\theta_{\text{HL}}$  (equivalently, the arrival time difference  $\Delta t_{\text{HL}}$ ).

#### 4. FOLLOW-UP OBSERVATIONS

Twenty-five participating teams of observers responded to the GW alert to mobilize satellites and ground-based telescopes spanning 19 orders of magnitude in EM wavelength. Observations and archival analysis started shortly after the candidate was announced, two days after the event was recorded. Most facilities followed tiling strategies based on the cWB and LIB sky maps. Some groups, considering the

possibility of a NS merger or core-collapse SN, selected fields based on the areal density of nearby galaxies or targeted the Large Magellanic Cloud (LMC) (e.g., [Annis et al. 2016](#)). Had the BBH nature of the signal been promptly available, most groups would not have favored local galaxies because LIGO’s range for BBH mergers is many times larger than that for BNSs. Fig. 3 displays the footprints of all reported observations. The campaign is summarized in Table 1 in terms of

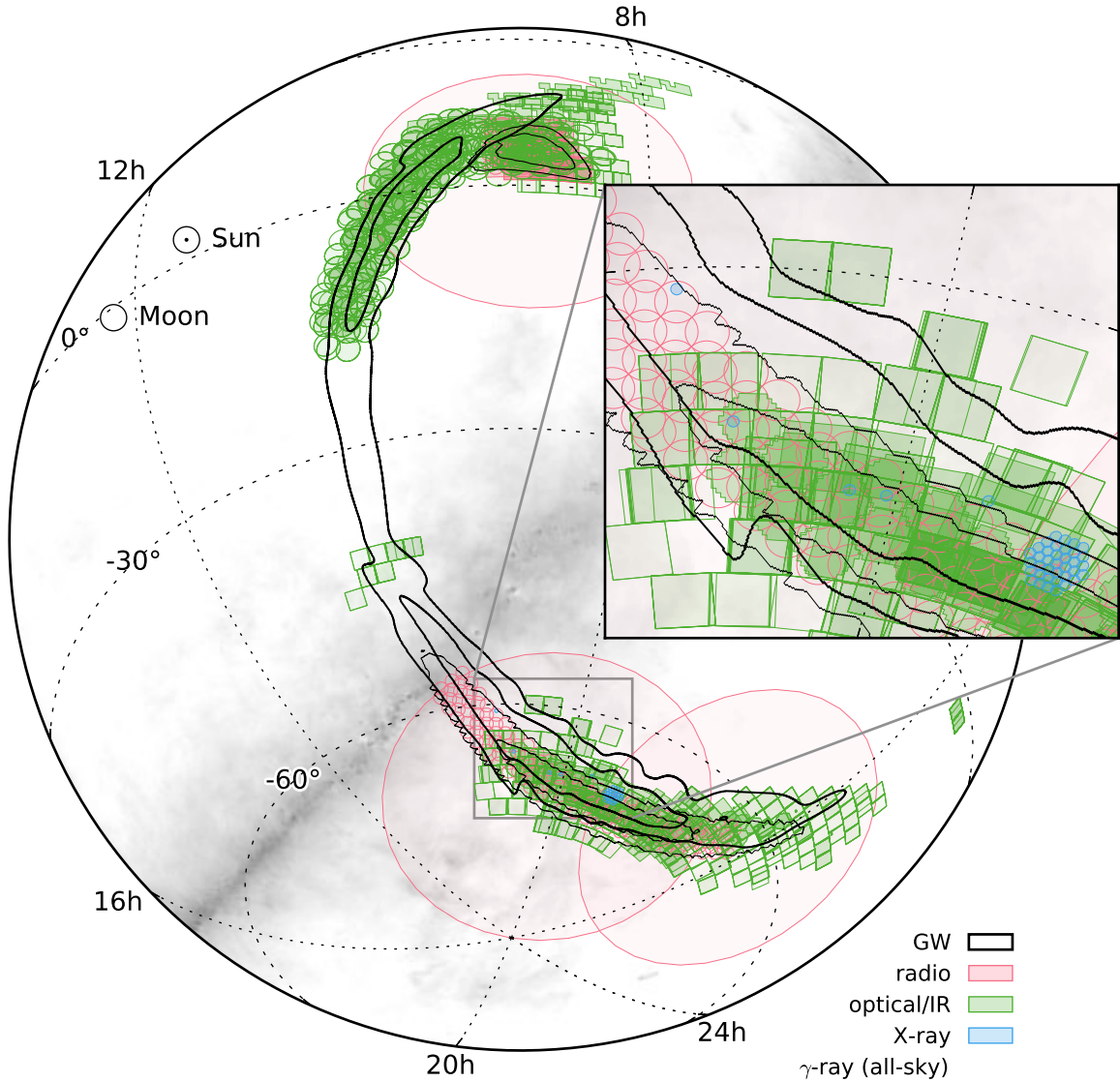


**Figure 3.** Footprints of observations in comparison with the 50% and 90% credible levels of the initially distributed GW localization maps. Radio fields are shaded in red, optical/infrared fields are in green, and the XRT fields are indicated by the blue circles. The all-sky *Fermi* GBM, LAT, *INTEGRAL* SPI-ACS, and MAXI observations are not shown. Where fields overlap, the shading is darker. The initial cWB localization is shown as thin black contour lines and the LIB localization as thick black lines. The inset highlights the *Swift* observations consisting of a hexagonal grid and a selection of the *a posteriori* most highly ranked galaxies. The [Schlegel et al. \(1998\)](#) reddening map is shown in the background to represent the Galactic plane. The projection is the same as in Fig. 2.

instruments, depth, time, and sky coverage. Some optical candidate counterparts were followed up spectroscopically and in the radio band as summarized in Table 2. The overall EM follow-up of GW150914 consisting of broad-band tiled ob-

servations and observations to characterize candidate counterparts are described in detail in Sections 3 through 5 of the Supplement ([Abbott et al. 2016g](#)).

Findings from these follow-up observations have been re-

ported in several papers. A weak transient signal was found in *Fermi* GBM data 0.4 s after the time of GW150914 (Connaughton et al. 2016), but no corresponding signal was found in the *INTEGRAL* SPI-ACS instrument (Savchenko et al. 2016) or *AGILE* (Tavani et al. 2016). No GRB-like afterglow was found in X-rays with *Swift* XRT (Evans et al. 2016) or MAXI (N. Kawai et al., in preparation), in UV/optical with *Swift* UVOT (Evans et al. 2016), or at GeV energies with *Fermi* LAT (Ackermann et al. 2016). Tiled observations with wide-field optical instruments listed in Table 1 found many transients, but spectroscopy with the instruments listed in Table 2 along with further photometry showed that none of them were associated with GW150914 (Kasliwal et al. 2016; Smartt et al. 2016; Soares-Santos et al. 2016; Morokuma et al. 2016). Annis et al. (2016) used DECAM to search for a missing supergiant in the LMC, which would have been evidence for the collapse of a massive star that could have produced GWs, but failed to produce a typical core-collapse SN.

## 5. COVERAGE

Using the GW data alone, we can only constrain the position of the source on the sky to an area of  $\approx 600 \text{ deg}^2$  (90% confidence). The inferred redshift is  $z = 0.09_{-0.04}^{+0.03}$ , corresponding to a luminosity distance of  $410_{-180}^{+160} \text{ Mpc}$  (Abbott et al. 2016e).

Table 1 lists the area tiled by each facility and the probability contained within those tiles, calculated with respect to the localization methods described in Section 3.

By far the most complete coverage of the area is at the highest energies. The *INTEGRAL* SPI-ACS provided the largest effective area in the 75 keV–1 MeV range, albeit with significantly varying detection efficiency. Owing to its nearly omnidirectional response, it had a full coverage of the GW probability map (GCN 18354; Savchenko et al. 2016). *Fermi* GBM captured 75% of the localization at the time of the GW trigger and the entire area by 25 minutes after (GCN 18339). *Fermi* LAT observations started 4200 s after the trigger and the entire localization continued to be observed every three hours.

Coverage in X-rays is complete down to  $10^{-9} \text{ erg cm}^{-2} \text{ s}^{-1}$  with the MAXI observations, but relatively sparse at fainter flux, with the *Swift* XRT tiles spanning about  $5 \text{ deg}^2$  and enclosing a probability of  $\sim 0.3\%$  in the energy range 0.3–10 keV to a depth of  $10^{-13}$ – $10^{-11} \text{ erg cm}^{-2} \text{ s}^{-1}$  (GCNs 18331, 18346).

Optical facilities together tiled about  $900 \text{ deg}^2$  and captured a containment probability of over 50% of the initial LIB sky map and slightly less for the final LALInference sky map that was available after the observations were completed. The depth varies widely among these facilities. MASTER and Pan-STARRS1 covered the most area with their observations, while large areas also were covered by the intermediate Palomar Transient Factory (iPTF), Dark Energy Camera (DECAM), VLT Survey Telescope (VST@ESO; E. Brocato et al. 2016, in preparation), and La Silla–QUEST. The contained

probability of the initial sky maps is dominated by MASTER, DECAM, Pan-STARRS1, La Silla–QUEST, and VST@ESO, while the final sky map is contained best by MASTER, DECAM and VST@ESO. Relatively small area and contained probability were covered by facilities that targeted nearby galaxies. The only wide-field near-infrared facility, the Visible and Infrared Survey Telescope (VISTA@ESO), covered  $70 \text{ deg}^2$  and captured a containment probability of 8% of the final LALInference sky map.

The radio coverage is also extensive, with a contained probability of 86%, dominated by Murchison Widefield Array (MWA) in the 118 MHz band (GCN 18345).

Table 2 lists the observations done by large telescope spectrographs and a radio facility to follow-up candidate optical counterparts. Deep photometry, broadband observations, and spectroscopy identified the majority of the candidates to be normal population type Ia and type II SNe, with a few dwarf novae and active galactic nuclei (AGNs) that are all very likely unrelated to GW150914. Candidate classification, comparison of redshift with the GW distance, and use of source age are crucial constraints to rule candidates in and out. Detailed discussions of candidate selection, spectroscopic and broadband follow-up are presented in survey-specific publications about iPTF candidates (Kasliwal et al. 2016) and about PESSTO follow-up of Pan-STARRS1 candidates (Smartt et al. 2016).

## 6. SENSITIVITY

The third column of Table 1 summarizes the depth of the follow-up program. We provide limiting flux, flux density, or magnitude for the different facilities. We emphasize that these limits only apply to the fraction of the sky contours that have been followed up. For example, the MWA fields have an 86% chance of containing the source’s sky location and provide no constraints on sky locations representing the remaining 14%.

Because the follow-up program was primarily designed to search for counterparts to BNS and NSBH mergers, it is interesting to note that the observational campaign would have provided powerful constraints on such a system. A BNS coalescence could have been detected by LIGO during O1 at a distance of  $\sim 70 \text{ Mpc}$ , averaged over sky position and orientations (Martynov et al. 2016). A short GRB afterglow similar to those that have been observed by *Swift* XRT would have been detectable at that distance. Re-scaling the observed X-ray fluxes of short GRBs at 11 hr after the event would yield fluxes in the range  $2 \times 10^{-11}$  to  $6 \times 10^{-8} \text{ erg cm}^{-2} \text{ s}^{-1}$  (Berger 2014). Kilonova emission from a BNS merger at that distance would reach a peak apparent magnitude of 17–24 within a week or two after the merger (e.g., Metzger et al. 2010; Barnes & Kasen 2013; Tanaka & Hotokezaka 2013; Grossman et al. 2014). This range overlaps with the depth reached in the optical and near-IR bands. Finally, this BNS system might produce radio emission from tens of  $\mu\text{Jy}$  to tens of mJy (e.g., Hotokezaka & Piran 2015) with different timescales spanning

**Table 1.** Summary of Tiled Observations

| Facility/<br>Instrument | Band <sup>a</sup>          | Depth <sup>b</sup>                            | Time <sup>c</sup> | Area<br>(deg <sup>2</sup> ) | Contained Probability (%) |      |                   |        | GCN                        |
|-------------------------|----------------------------|---|-------------------|-----------------------------|---------------------------|------|-------------------|--------|----------------------------|
|                         |                            |   |                   |                             | cWB                       | LIB  | BSTR <sup>d</sup> | LALInf |                            |
| Gamma-ray               |                            |   |                   |                             |                           |      |                   |        |                            |
| <i>Fermi</i> LAT        | 20 MeV–<br>300 GeV         | $1.7 \times 10^{-9}$                          | (every<br>3 hr)   | —                           | 100                       | 100  | 100               | 100    | 18709                      |
| <i>Fermi</i> GBM        | 8 keV–40 MeV               | $0.7\text{--}5 \times 10^{-7}$<br>(0.1–1 MeV) | (archival)        | —                           | 100                       | 100  | 100               | 100    | 18339                      |
| INTEGRAL                | 75 keV–1 MeV               | $1.3 \times 10^{-7}$                          | (archival)        | —                           | 100                       | 100  | 100               | 100    | 18354                      |
| IPN                     | 15 keV–10 MeV              | $1 \times 10^{-7}$                            | (archival)        | —                           | 100                       | 100  | 100               | 100    | —                          |
| X-ray                   |                            |   |                   |                             |                           |      |                   |        |                            |
| MAXI/GSC                | 2–20 keV                   | $1 \times 10^{-9}$                            | (archival)        | 17900                       | 95                        | 89   | 92                | 84     | 19013                      |
| <i>Swift</i> XRT        | 0.3–10 keV                 | $5 \times 10^{-13}$ (gal.)                    | 2.3, 1, 1         | 0.6                         | 0.03                      | 0.18 | 0.04              | 0.05   | 18331                      |
|                         |                            | $2\text{--}4 \times 10^{-12}$ (LMC)           | 3.4, 1, 1         | 4.1                         | 1.2                       | 1.9  | 0.16              | 0.26   | 18346                      |
| Optical <sup>e</sup>    |                            |   |                   |                             |                           |      |                   |        |                            |
| DECam                   | <i>i, z</i>                | $i < 22.5, z < 21.5$                          | 3.9, 5, 22        | 100                         | 38                        | 14   | 14                | 11     | 18344, 18350               |
| iPTF                    | <i>R</i>                   | $R < 20.4$                                    | 3.1, 3, 1         | 130                         | 2.8                       | 2.5  | 0.0               | 0.2    | 18337                      |
| KWFC                    | <i>i</i>                   | $i < 18.8$                                    | 3.4, 1, 1         | 24                          | 0.0                       | 1.2  | 0.0               | 0.1    | 18361                      |
| MASTER                  | <i>C</i>                   | $< 19.9$                                      | -1.1, 7, 7        | 710                         | 50                        | 36   | 55                | 50     | 18333, 18390, 18903, 19021 |
| Pan-STARRS1             | <i>i</i>                   | $i < 19.2\text{--}20.8$                       | 3.2, 21, 42       | 430                         | 28                        | 29   | 2.0               | 4.2    | 18335, 18343, 18362, 18394 |
| La Silla–<br>QUEST      | <i>g, r</i>                | $r < 21$                                      | 3.8, 5, 0.1       | 80                          | 23                        | 16   | 6.2               | 5.7    | 18347                      |
| SkyMapper               | <i>i, v</i>                | $i < 19.1, v < 17.1$                          | 2.4, 2, 3         | 30                          | 9.1                       | 7.9  | 1.5               | 1.9    | 18349                      |
| <i>Swift</i> UVOT       | <i>u</i>                   | $u < 19.8$ (gal.)                             | 2.3, 1, 1         | 3                           | 0.7                       | 1.0  | 0.1               | 0.1    | 18331                      |
|                         |                            | $u < 18.8$ (LMC)                              | 3.4, 1, 1         |                             |                           |      |                   |        | 18346                      |
| TAROT                   | <i>C</i>                   | $R < 18$                                      | 2.8, 5, 14        | 30                          | 15                        | 3.5  | 1.6               | 1.9    | 18332, 18348               |
| TOROS                   | <i>C</i>                   | $r < 21$                                      | 2.5, 7, 90        | 0.6                         | 0.03                      | 0.0  | 0.0               | 0.0    | 18338                      |
| VST@ESO                 | <i>r</i>                   | $r < 22.4$                                    | 2.9, 6, 50        | 90                          | 29                        | 10   | 14                | 10     | 18336, 18397               |
| Near Infrared           |                            |   |                   |                             |                           |      |                   |        |                            |
| VISTA@ESO               | <i>Y, J, K<sub>S</sub></i> | $J < 20.7$                                    | 4.8, 1, 7         | 70                          | 15                        | 6.4  | 10                | 8.0    | 18353                      |
| Radio                   |                            |   |                   |                             |                           |      |                   |        |                            |
| ASKAP                   | 863.5 MHz                  | 5–15 mJy                                      | 7.5, 2, 6         | 270                         | 82                        | 28   | 44                | 27     | 18363, 18655               |
| LOFAR                   | 145 MHz                    | 12.5 mJy                                      | 6.8, 3, 90        | 100                         | 27                        | 1.3  | 0.0               | 0.1    | 18364, 18424, 18690        |
| MWA                     | 118 MHz                    | 200 mJy                                       | 3.5, 2, 8         | 2800                        | 97                        | 72   | 86                | 86     | 18345                      |

<sup>a</sup>Band: photon energy, optical or near-infrared filter (or C for clear unfiltered light), wavelength range, or central frequency.

<sup>b</sup>Depth: gamma/X-ray limiting flux in  $\text{erg cm}^{-2} \text{s}^{-1}$ ;  $5\sigma$  optical/IR limiting magnitude (AB); and  $5\sigma$  radio limiting spectral flux density in mJy. The reported values correspond to the faintest flux/magnitude of detectable sources in the images.

<sup>c</sup>Elapsed time in days between start of observations and the time of GW150914 (2015 September 14 09:50:45), number of repeated observations of the same area, and total observation period in days.

<sup>d</sup>BAYESTAR.

<sup>e</sup>Searches for bright optical transients were also done by BOOTES-3 and Pi of the Sky. Details are given in the Supplement (Abbott et al. 2016g).

**Table 2.** Summary of Follow-up Observations

| Spectroscopic Follow-up |                   |                   |        |               |                              |   |
|-------------------------|-------------------|-------------------|--------|---------------|------------------------------|---|
| Instrument              | No. of Candidates | Discovery Survey  | Epochs | $\lambda$ (Å) | $\Delta\lambda^a$ (Å)        | GCN   |
| KeckII+DEIMOS           | 8                 | iPTF              | 1      | 4650 – 9600   | 3.5                          | <a href="#">18337</a> , <a href="#">18341</a>                         |
| LT+SPRAT                | 1                 | Pan-STARRS1       | 1      | 4500 – 7500   | 18                           | <a href="#">18370</a> , <a href="#">18371</a>                         |
| NTT+EFOSC2              | 10                | QUEST/Pan-STARRS1 | 1      | 3650 – 9250   | 18                           | <a href="#">18359</a> , <a href="#">18395</a>                         |
| P200+DBSP               | 1                 | Pan-STARRS1       | 1      | 3200 – 9000   | 4 – 8                        | <a href="#">18372</a>   |
| UH2.2m+SNIFS            | 9                 | Pan-STARRS1       | 1      | 3200 – 10000  | 4 – 6                        | —   |
| Radio Follow-up         |                   |                   |        |               |                              |   |
| Instrument              | No. of Candidates | Discovery Survey  | Epochs | Freq. (GHz)   | Lim. Flux <sup>b</sup> (uJy) | GCN   |
| VLA                     | 1                 | iPTF              | 3      | 6             | $\lesssim 50$                | <a href="#">18420</a> , <a href="#">18474</a> , <a href="#">18914</a> |

<sup>a</sup>Full width at half maximum resolution.

<sup>b</sup> $5\sigma$ , 2 GHz nominal bandwidth,  $\approx 20$  min on-source.



weeks to years. Tables 1 and 2 show that the radio observations from wide-field facilities were sensitive to mJy flux densities at low frequencies where fainter sources with longer timescales are expected, while the narrow-field VLA was sensitive to well localized radio transients down to  $\mu\text{Jy}$  flux densities at frequencies above a few GHz.

## 7. CONCLUSIONS

GW150914 is consistent with the inspiral and merger of two BHs of masses  $36_{-4}^{+5}$  and  $29_{-4}^{+4} M_{\odot}$ , respectively, resulting in the formation of a final BH of mass  $62_{-4}^{+4} M_{\odot}$  (Abbott et al. 2016c). In classical general relativity, a vacuum BBH merger does not produce any EM or particle emission whatsoever. Whereas supermassive BBHs in galactic centers may appear as dual AGNs or have other distinctive EM signatures due to interactions with gas or magnetic fields, stellar BBH systems are not expected to possess detectable EM counterparts. The background gas densities and magnetic field strengths should therefore be typical of the interstellar medium, which are many orders of magnitude smaller than the environments of EM bright supermassive BBHs. Although GW150914 is loud in GWs and expected to be absent in all EM bands, thorough follow-up observations were pursued to check for EM emission. Future EM follow-ups of GW sources will shed light on the presence or absence of firm EM counterparts and astrophysical processes that may trigger EM emission from these systems.

The EM campaign following GW150914 successfully demonstrates the capability of the observing partners to cover large swaths of the sky localization area, to identify candidates, and to activate larger telescopes for photometric and spectroscopic characterization within a few days of an event. We note that the information about the source's BBH nature and updated sky maps were sent out 20 days and four months after the event, respectively. This resulted in some instruments covering much less of the probability region or to the required depth of GW150914 than they may have planned for. We expect future alerts to be issued within tens of minutes with more information about the signal type and more rapid updates of the maps. The follow-up efforts would have been sensitive to a wide range of emission expected from BNS or NSBH mergers. However, the widely variable sensitivity reached across the sky localization area continues to be a challenge for an EM counterpart search.

The number of galaxies (with luminosities  $L \geq 0.1L^*$ ; Blanton et al. 2003) within the comoving volume of  $10^{-2} \text{ Gpc}^3$  corresponding to the 90% credible area of the LALInference sky map and within the 90% confidence interval distance is  $\sim 10^5$ . Such a number makes it impossible to identify the host galaxy in the absence of an EM counterpart detection. The presence of a third GW detector such as Virgo would have improved the sky localization of GW150914 to a few tens of square degrees both for the unmodeled and CBC searches. The future addition of more GW detectors to the global net-

work (Abbott et al. 2016f) will significantly improve the efficiency of searches for EM counterparts.

In summary, we have described the EM follow-up program carried out for the first GW source detected by Advanced LIGO. Within two days of the initial tentative detection of GW150914, a GCN circular was sent to EM follow-up partners alerting them to the event and providing them with initial sky maps. Twenty-five EM observing teams mobilized their resources, and over the ensuing three months observations were performed with a diverse array of facilities over a broad wavelength range (from radio to  $\gamma$ -ray). Findings from those observations are being disseminated in other papers. The localization and broadband follow-up of this GW event constitutes an important first step in a new era of gravitational wave multi-messenger astronomy.

See the Supplement (Abbott et al. 2016g) for a full list of acknowledgements. This is LIGO document LIGO-P1500227-v12.

## REFERENCES

- Aasi, J., Abadie, J., Abbott, B. P., et al. 2014, *ApJS*, 211, 7  
Aasi, J., Abbott, B. P., Abbott, R., et al. 2015, *Classical and Quantum Gravity*, 32, 074001  
Abadie, J., Abbott, B. P., Abbott, R., et al. 2012a, *A&A*, 541, A155  
— 2012b, *A&A*, 539, A124  
Abbott, B. P., Abbott, R., Abbott, T. D., et al. 2016a, *Class. Quantum Grav.*, 33, 134001  
— 2016b, *Phys. Rev. D*, 93, 122003  
— 2016c, *Phys. Rev. Lett.*, 116, 061102  
— 2016d, *Phys. Rev. D*, 93, 122004  
— 2016e, *Phys. Rev. Lett.*, 116, 241102,  
<https://dcc.ligo.org/LIGO-P1500218/public/main>  
— 2016f, *Living Reviews in Relativity*, 19, 1  
— 2016g, arXiv:1604.07864,  
<https://dcc.ligo.org/LIGO-P1600137/public/main>  
Acerese, F., Agathos, M., Agatsuma, K., et al. 2015, *Classical and Quantum Gravity*, 32, 024001  
Ackermann, M., Ajello, M., Albert, A., et al. 2016, *ApJL*, 823, L2  
Adams, T., Buskulic, D., Germain, V., et al. 2015, *ArXiv e-prints*, arXiv:1512.02864  
Annis, J., Soares-Santos, M., Berger, E., et al. 2016, *ApJL*, 823, L34  
Bannister, K., Marvil, J., Heywood, I., et al. 2015a, *GCN*, 18363, 1  
— 2015b, *GCN*, 18655, 1  
Barnes, J., & Kasen, D. 2013, *ApJ*, 775, 18  
Berger, E. 2014, *ARA&A*, 52, 43  
Blackburn, L., Briggs, M. S., Burns, E., et al. 2015, *GCN*, 18339, 1  
Blanton, M. R., Hogg, D. W., Bahcall, N. A., et al. 2003, *ApJ*, 592, 819  
Brocato, E., Branchesi, M., Campana, S., et al. 2015a, *GCN*, 18336, 1  
Brocato, E., Branchesi, M., Grado, A., et al. 2015b, *GCN*, 18397, 1  
Broderick, J., Jonker, P. G., Fender, R. P., et al. 2015a, *GCN*, 18364, 1  
— 2015b, *GCN*, 18424, 1  
Campbell, H., Lyman, J., Fraser, M., et al. 2015, *GCN*, 18395, 1  
Cannon, K., Cariou, R., Chapman, A., et al. 2012, *ApJ*, 748, 136  
Chambers, K., Huber, M., Magnier, E., et al. 2015, *GCN*, 18335, 1  
Colazo, C., Lambas, D. G., Sanchez, B., et al. 2015, *GCN*, 18338, 1  
Connaughton, V., Burns, E., Goldstein, A., et al. 2016, *ArXiv e-prints*, arXiv:1602.03920  
Eichler, D., Livio, M., Piran, T., & Schramm, D. N. 1989, *Nature*, 340, 126

- Essick, R., Vitale, S., Katsavounidis, E., Vedovato, G., & Klimenko, S. 2015, *ApJ*, 800, 81
- Evans, P. A., Kennea, J. A., Barthelmy, S., et al. 2015a, *GCN*, 18331, 1  
— 2015b, *GCN*, 18346, 1
- Evans, P. A., Fridriksson, J. K., Gehrels, N., et al. 2012, *ApJS*, 203, 28
- Evans, P. A., Kennea, J. A., Barthelmy, S. D., et al. 2016, *MNRAS*, arXiv:1602.03868
- Ferrigno, C., Savchenko, V., Mereghetti, S., et al. 2015, *GCN*, 18354, 1
- Fong, W., Berger, E., Margutti, R., & Zauderer, B. A. 2015, *ApJ*, 815, 102
- Grossman, D., Korobkin, O., Rosswog, S., & Piran, T. 2014, *MNRAS*, 439, 757
- Hansen, B. M. S., & Lyutikov, M. 2001, *MNRAS*, 322, 695
- Hotokezaka, K., & Piran, T. 2015, *MNRAS*, 450, 1430
- Kaplan, D., Croft, S., Bannister, K., et al. 2015, *GCN*, 18345, 1
- Kasliwal, M. M., Cenko, S. B., Cao, Y., et al. 2015, *GCN*, 18341, 1
- Kasliwal, M. M., & Nissanke, S. 2014, *ApJL*, 789, L5
- Kasliwal, M. M., Cenko, S. B., Singer, L. P., et al. 2016, *ArXiv e-prints*, arXiv:1602.08764
- Klimenko, S., Vedovato, G., Drago, M., et al. 2016, *Phys. Rev. D*, 93, 042004
- Klotz, A., & Boer, M. 2015a, *GCN*, 18332, 1  
— 2015b, *GCN*, 18348, 1
- Lattimer, J. M., & Schramm, D. N. 1976, *ApJ*, 210, 549
- Li, L.-X., & Paczyński, B. 1998, *ApJL*, 507, L59
- LIGO Scientific Collaboration, & Virgo. 2015a, *GCN*, 18330, 1  
— 2015b, *GCN*, 18388, 1  
— 2016a, *GCN*, 18858, 1  
— 2016b, *GCN*, 18851, 1
- Lipunov, V., Gorbvskoy, E., Tyurina, N., et al. 2015a, *GCN*, 18333, 1  
— 2016a, *GCN*, 19021, 1  
— 2016b, *GCN*, 18903, 1
- Lipunov, V. M., Gorbvskoy, E. S., Buckley, D., et al. 2015b, *GCN*, 18390, 1
- Lynch, R., Vitale, S., Essick, R., Katsavounidis, E., & Robinet, F. 2015, *ArXiv e-prints*, arXiv:1511.05955
- Martynov, D. V., Hall, E. D., Abbott, B. P., et al. 2016, *ArXiv e-prints*, arXiv:1604.00439
- Messick, C., Blackburn, K., Brady, P., et al. 2016, *ArXiv e-prints*, arXiv:1604.04324
- Metzger, B. D., Martínez-Pinedo, G., Darbha, S., et al. 2010, *MNRAS*, 406, 2650
- Morokuma, T., Tanaka, M., Yoshida, M., et al. 2015, *GCN*, 18361, 1
- Morokuma, T., Tanaka, M., Asakura, Y., et al. 2016, *ArXiv e-prints*, arXiv:1605.03216
- Nakar, E. 2007, *Phys. Rep.*, 442, 166
- Nakar, E., & Piran, T. 2011, *Nature*, 478, 82
- Narayan, R., Paczynski, B., & Piran, T. 1992, *ApJL*, 395, L83
- Omodei, N., McEnery, J., & Vianello, G. 2015, *GCN*, 18709, 1
- Palliyaguru, N., & Corsi, A. 2015a, *GCN*, 18420, 1  
— 2015b, *GCN*, 18474, 1  
— 2016, *GCN*, 18914, 1
- Rabinowitz, D., Baltay, C., Ellman, N., et al. 2015, *GCN*, 18347, 1
- Rowlinson, A., Broderick, J., Jonker, P., et al. 2015, *GCN*, 18690, 1
- Savchenko, V., Ferrigno, C., Mereghetti, S., et al. 2016, *ApJL*, 820, L36
- Schlegel, D. J., Finkbeiner, D. P., & Davis, M. 1998, *ApJ*, 500, 525
- Serino, M., Negoro, H., Kawai, N., et al. 2016, *GCN*, 19013, 1
- Singer, L. P., Kasliwal, M. M., Cenko, S. B., et al. 2015, *GCN*, 18337, 1
- Singer, L. P., & Price, L. R. 2016, *Phys. Rev. D*, 93, 024013
- Singer, L. P., Price, L. R., Farr, B., et al. 2014, *ApJ*, 795, 105
- Smartt, S. J., Kupfer, T., Chambers, K., et al. 2015a, *GCN*, 18372, 1
- Smartt, S. J., Smith, K. W., Chambers, K., et al. 2015b, *GCN*, 18362, 1  
— 2015c, *GCN*, 18394, 1  
— 2015d, *GCN*, 18343, 1
- Smartt, S. J., Chambers, K. C., Smith, K. W., et al. 2016, *ArXiv e-prints*, arXiv:1602.04156
- Soares-Santos, M., Annis, J., Berger, E., et al. 2015a, *GCN*, 18344, 1  
— 2015b, *GCN*, 18350, 1
- Soares-Santos, M., Kessler, R., Berger, E., et al. 2016, *ApJL*, 823, L33
- Steele, I. A., Copperwheat, C. M., Piascik, A. S., et al. 2015a, *GCN*, 18370, 1  
— 2015b, *GCN*, 18371, 1
- Takats, K., Agliozzo, C., Razza, A., et al. 2015, *GCN*, 18359, 1
- Tanaka, M., & Hotokezaka, K. 2013, *ApJ*, 775, 113
- Tanvir, N. R., Levan, A. J., White, D., et al. 2015, *GCN*, 18353, 1
- Tavani, M., Pittori, C., Verrecchia, F., et al. 2016, *ArXiv e-prints*, arXiv:1604.00955
- Veitch, J., Raymond, V., Farr, B., et al. 2015, *Phys. Rev. D*, 91, 042003
- Yuan, F., Wolf, C., Scalzo, R., & Schmidt, B. 2015, *GCN*, 18349, 1
- Zhang, B. 2014, *ApJL*, 780, L21